TECHNICAL MEMORANDUM

ALL-METAL, COMPACT HEAT EXCHANGER FOR SPACE CRYOCOOLERS

TM-1450

NOVEMBER 1990

Creare

ALL-METAL, COMPACT HEAT EXCHANGER FOR SPACE CRYOCOOLERS

by

Walter L. Swift
Javier Valenzuela
Herbert Sixsmith

Creare Inc.
P.O. Box 71
Hanover, NH 03755

September 1990
Final Report for Period September 1987 - June 1990

Prepared for

GODDARD SPACE FLIGHT CENTER
Greenbelt, MD 20771

NASA CONTRACT NAS5-30172

NASA National Aeronautics and Space Administration

Report Documentation Page

1. Report No.	2. Government Accession No.	3. Recipient's Catalog No.

4. Title and Subtitle
ALL-METAL, COMPACT HEAT EXCHANGER FOR SPACE CRYOCOOLERS

5. Report Date
September 1990

6. Performing Organization Code

7. Author(s)
Swift, Walter L.

8. Performing Organization Report No.
TM-1450

10. Work Unit No.

9. Performing Organization Name and Address
Creare Inc.
P.O. Box 71
Hanover, NH 03755

11. Contract or Grant No.
NASS-30172

13. Type of Report and Period Covered
Final Report
Period Sept. 87 - Jun 90

12. Sponsoring Agency Name and Address
NASA Goddard Space Flight Center
Max Gasser, Code 713.1
Greenbelt, MD 20771

14. Sponsoring Agency Code

15. Supplementary Notes

16. Abstract

This report describes the development of a high performance, all metal compact heat exchanger. The device is designed for use in a reverse Brayton cryogenic cooler which provides five watts of refrigeration at 70 K. The heat exchanger consists of a stainless steel tube concentrically assembled within a second stainless steel tube. Approximately 300 pairs of slotted copper disks and matching annular slotted copper plates are positioned along the centerline axis of the concentric tubes. Each of the disks and plates has approximately 1200 precise slots machined by means of a special electric discharge process. Positioning of the disk and plate pairs is accomplished by means of dimples in the surface of the tubes. Mechanical and thermal connections between the tubes and plate/disk pairs are made by solder joints.

The heat exchanger assembly is 9 cm in diameter by 50 cm in length and has a mass of 10 kg. The predicted thermal effectiveness is greater than 0.985 at design conditions. Pressure loss at design conditions is less than 5 kPa in both fluid passages. Tests were performed on a subassembly of plates integrally soldered to two end headers. The measured thermal effectiveness of the test article exceeded predicted levels. Pressure losses were negligibly higher than predictions.

17. Key Words (Suggested by Author(s))	18. Distribution Statement
cryogenics, heat exchanger, cryocooler, thermal effectiveness	

19. Security Classif. (of this report)	20. Security Classif. (of this page)	21. No. of pages	22. Price
Unclassified	Unclassified	32	

NASA FORM 1626 OCT 86

Creare

PROPRIETARY NOTICE

This SBIR data is furnished with SBIR rights under NASA Contract No. NAS5-30172. For a period of 2 years after acceptance of all items to be delivered under this contract the Government agrees to use this data for Government purposes only, and it shall not be disclosed outside the Government (including disclosure for procurement purposes) during such period without permission of the Contractor, except that, subject to the foregoing use and disclosure prohibitions, such data may be disclosed for use by support contracts. After the aforesaid 2-year period the Government has a royalty-free license to use, and to authorize others to use on its behalf, this data for Government purposes, but is relieved of all disclosure prohibitions and assumes no liability for unauthorized use of this data by third parties. This notice shall be affixed to any reproductions of this data in whole or in part.

Creare

PREFACE

This report describes the development of a high performance, all metal, compact heat exchanger for use in a reverse Brayton cryogenic cycle. The objective was to attain very high thermal effectiveness with low pressure losses in an all - metal design which could be used for long life space applications. Key features of the device are compactness and light weight which are important in space systems. The heat exchanger was targeted for a specific 5 watt cryocooler. However, the design methods and fabrication techniques can be used for a range of cryogenic applications.

The work performed during this two phase SBIR project included performance modelling and preliminary design in Phase I, and detailed modelling, detailed design, fabrication technology development, and testing in Phase II.

In Phase I, preliminary performance models were used to parametrically evaluate heat exchanger performance as a function of geometry. Two concepts were studied - a perforated plate design and a pleated foil geometry. The effects of slot and hole geometry, number, plate number and thickness, materials, etc. were evaluated with respect to fabrication approaches which could yield optimal performance in the perforated plate configuration. A pleated foil concept was also devised and assessed in terms of performance and fabricability. A slotted plate configuration which could achieve the performance targets was selected for further development. This configuration appeared to have a higher likelihood of success in terms of fabrication risks - though the pleated foil concept had a significant advantage in size and weight at comparable performance levels.

Three important fabrication challenges were identified, and approaches to meeting these challenges were proposed. The challenges were:

1) Automated slot fabrication. High performance depends on accurate machining of more than a million slots in the disks and plates.

2) Precision positioning of disk and annular plate pairs. Axial misalignment between matching disk and plate pairs produces a significant penalty in heat transfer.

3) Bonding. Soldering materials and techniques determine structural and thermal performance.

A plan for the development of the heat exchanger was proposed which included development of the fabrication methods, and construction and testing of a heat exchanger in Phase II.

In Phase II, the design and modelling effort were iterated with developments in fabrication methods. The modelling effort focused on correct representation of the relative effects of the loss mechanisms on overall performance. The heat exchanger is a counterflow design, where high pressure gas flows through slots in disks which are axially positioned along a center tube. Heat flows from the gas to the plates, through the plates to the wall of the tube, through the tube wall to matching annular plates which are contained within an outer tube. These plates also have slots through which the low pressure stream flows carrying away the heat transmitted from the high pressure stream.

Creare

Features of the design which are important to performance and size include number and sizes of slots, number of plates, conductivity of the plates, thermal resistivity of the tubes, and thermal and mechanical integrity of the joints between plates and tubes. Other features which are also important include the structural integrity of the assembly, cleanliness (elimination of contaminants), size, weight and fabricability. Compromises between these features and issues were required in order to produce a heat exchanger which met competing requirements.

A major portion of the Phase II effort involved the development and refinement of fabrication methods which would ensure that the heat exchanger could be built. The most important Phase II accomplishments were:

1) An automated technique for precision cutting of thousands of small slots was successfully demonstrated,

2) Methods for soldering of the plate and tube assembly were successfully established and demonstrated,

3) A mechanical fixturing and indexing device for precise positioning of disks and plates was developed, and

4) A heat exchanger test article was fabricated using the techniques listed above, and tests showed that the unit's performance was better than the model predictions.

A goal of the original program plan had been to fabricate a complete 300 plate-pair heat exchanger and test it at cryogenic temperatures. This goal was not met. We devoted more effort than originally planned toward the required fabrication technologies at the expense of building a full - up heat exchanger assembly for cryogenic testing. This strategy was followed to reduce the risk of not meeting technical performance objectives of the project. Specifically, in the final stages of assembly of the disks and plates within the tubes, it was found that our initial approach for positioning the disk and plate pairs was not reliable. Subassembly soldering trials showed that some plates and disks moved slightly during the soldering process. If we chose to proceed with fabrication of a complete heat exchanger assembly using this process, the performance goals would not be met. We instead devised a method for positive positioning of plates and disks, built the required tooling and fabricated and assembled a test article consisting of 14 plates. Accurate tests were performed and results compared with the thermal model used to design the heat exchanger. These comparisons showed that the test results exceeded predicted performance levels.

These results are very encouraging. The thermal model was upgraded to remove some simplifying assumptions used in the early version and the agreement between data and predictions was excellent. The upgraded model shows that the performance of the heat exchanger for use in the cryocooler will be better than the design goals. The original goal for thermal effectiveness was 0.985. The current prediction based on test results is that the effectiveness may be as high as 0.993. Pressure losses are predicted to be the same as original targets.

The results of this effort indicate that the high performance design can be successfully built and that the original performance targets can be met. A heat exchanger of this type for use in a cryocooler to supply 5 W of refrigeration at 70 K should have an overall mass of about 5 kg and a package envelope of 9 cm diameter x 50 cm length. Subassembly tests on

Creare

mockups have shown that the mechanical integrity of the solder joints is good. However, detailed structural design and analyses must be performed to establish the support requirements and means for high vibration load situations (such as launch). A complete assembly should be built to verify actual performance at cryogenic temperatures.

TABLE OF CONTENTS

Creare

LIST OF FIGURES

LIST OF TABLES

Creare

1. INTRODUCTION

This report describes the results of a two phase program to develop a high performance, all - metal heat exchanger for cryogenic applications. The project was sponsored by NASA/GSFC under the Small Business Innovation Research Program. The period of performance was January 1986 - June 1986 for Phase I and September 1987 - June 1990 for Phase II. The Technical Monitor for NASA/GSFC was Max Gasser. Key individuals at Creare included:

Dr. Herbert Sixsmith - Principal Investigator

Mr. Walter Swift - Project Director

Dr. Javier Valenzuela - Project Engineer

Mr. Matthew Miller - Project Engineer

After this introduction with comments about the cycle for which the heat exchanger is designed, the report is divided into five technical sections. The first (Design Goals) presents a summary of the requirements and specifications which were assumed and adopted to guide the development of the unit. The next section (Heat Exchanger Design) discusses the mechanical and thermal design of the device. Following this is a section on Fabrication Issues which includes descriptions of the developments during this project. The section on Thermal Modelling discusses key features of the models used to optimize the design and to finally compare test results with predictions. The section on Testing discusses the test article, measurements, test results and comparisons with predictions. The section also presents a discussion of the implications of the results on the performance of a full up device for the baseline cryocooler. Finally, the Conclusions from this effort are summarized in the last section.

1.1 Background

Three important requirements for mechanical cryogenic coolers intended for use in long life space applications are:

- reliability - significant degradation or failure of the system is generally unacceptable,
- low vibration - many missions involve cooling for sensors where significant levels of mechanical vibration are unacceptable, and
- performance - thermodynamic performance of the system strongly impacts overall payload launch weight.

Mechanical coolers using turbomachines in a reverse Brayton cycle have the potential to meet each of the above requirements for certain loads and temperatures. The current state of technology is such that for refrigeration capacities above about 3 W for temperatures between 4 K and 100 K, performance levels for turbo Brayton type cycles make them prime candidates for use in such applications. For lower capacities, Stirling type coolers appear to be more attractive.

Creare

An important reason for the unattractiveness of turbo Brayton cycles below about 3 W is that the overall cycle performance levels decrease rapidly as refrigeration capacities decrease. This is basically a scale effect, where efficiencies of cycle components decrease with size. In order to extend the range of high performance levels to lower refrigeration capacities for this type cycle, technology improvements must occur - those which will result in higher efficiencies at smaller scales.

There are four basic components to turbo Brayton cycles: the turbine which produces useful refrigeration, a heat exchanger which precools high pressure gas to be expanded through the turbine, a compressor which produces the necessary pressure difference for expansion and a power converter which drives the compressor. The efficiencies of each of these components are important, but changes in efficiencies of the components which operate at low temperature tend to have a larger per unit impact on overall cycle performance. Furthermore, the components which operate at low temperature ends of the cycle tend to be more challenging because of their reduced size. Within a given cycle, machines operating with high density fluid will be generally smaller than the low density devices. The key to achieving high efficiency at reduced refrigeration capacities is in the ability to fabricate with precision in very small sizes.

This effort is one of several projects to develop technology for increasing performance of low capacity cryocoolers. The heat exchanger was addressed because it has a significant effect on overall efficiency of the reverse Brayton cycle, particularly where turbomachines are used. The goals for the development were to achieve very high thermal effectiveness with low pressure loss using all metal construction in a compact configuration. A particular cycle and refrigeration requirement served to focus the effort. However, the objective was to develop the technology to be used over a range of sizes and applications.

The cycle is shown schematically in Figure 1.1. This is a Single Stage Reverse Brayton cycle consisting of the compressor, heat exchanger and turbine. At the warmer end of the cycle, work is required for compression of the fluid, and heat is rejected. At the cold end, work is extracted from the fluid and heat is absorbed from a load. The cycle design point operating conditions are shown on the Figure.

Several references [1], [2], [3] describe the cycle and early work which was used to establish preliminary design targets and features of the heat exchanger. During Phase II of this project, the preliminary values were refined in light of practical limitations in fabrication processes which were under development. Our approach was to set very challenging targets for the device in terms of performance, weight, size, etc. at the outset, establish physical requirements on the basis of these targets, then to compromise in fabrication only when it was absolutely necessary to assure that the device could be produced. As a result, there are some slight inconsistencies between data and geometry details which appear in early reports and the final configuration. However, the performance targets were met. In fact, test results showed better performance than were predicted in the thermal model used to design the heat exchanger.

Creare

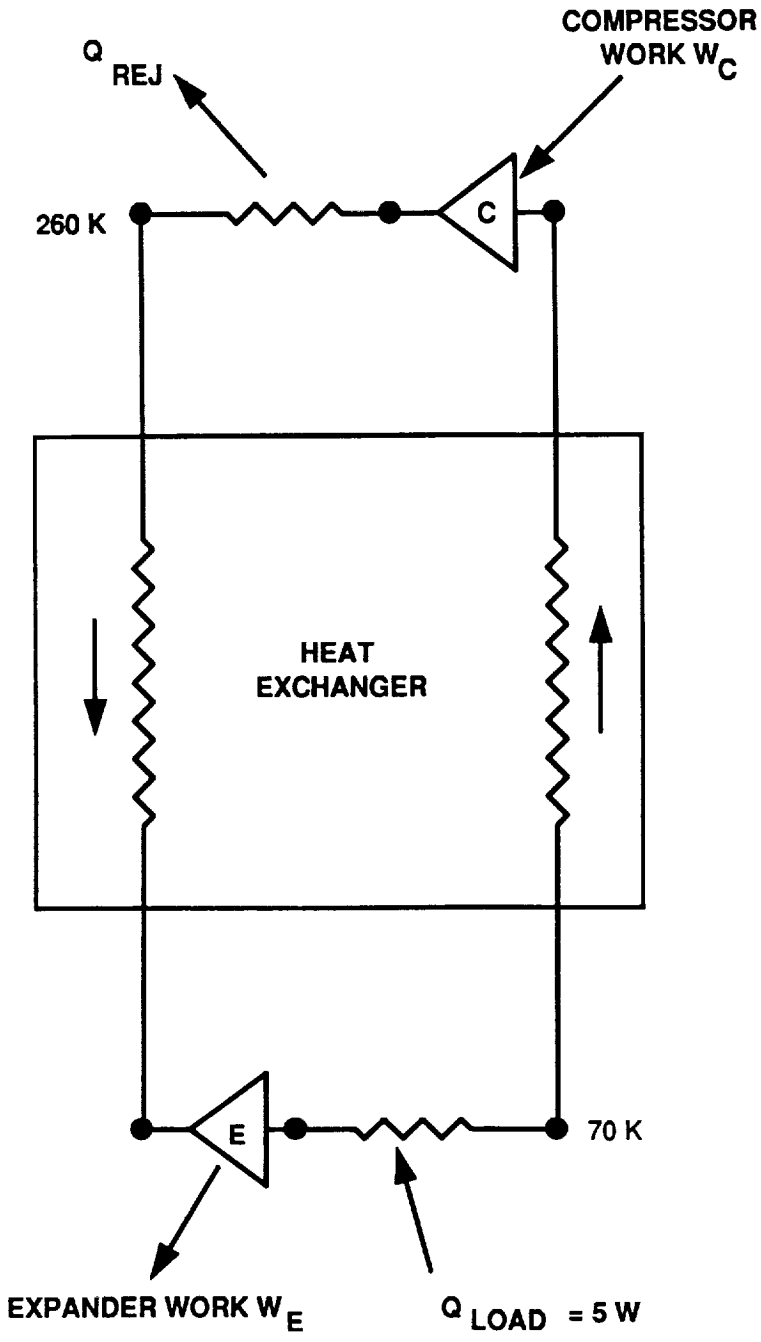

Figure 1.1 SCHEMATIC OF THE SINGLE STAGE REVERSE BRAYTON CRYOCOOLER

Creare

2. DESIGN GOALS

The heat exchanger specifications were based on requirements in a cryocooler for a long life mission in space with a cooling capacity of 5 W at 70 K. The goal for the cycle was to develop components in order that an overall performance target of 30 W input power per watt of refrigeration could be met at these conditions. The reverse Brayton cycle was chosen, and the compressor and expander within the cycle were turbomachines. Using these fairly broad requirements, an optimization study was performed to characterize the relative importance of individual component features and efficiencies [1], [2], [3]. These studies incorporated practical limitations in current technology as part of the considerations in arriving at target performance levels. Each of the components (the turbine, compressor, heat exchanger and controller) was evaluated. Performance requirements which were achievable with some technology development were established for each. The results were combined in a way which would yield the overall cycle performance which was desired.

The output from the analysis and modelling effort was a set of specifications for the cycle which included performance requirements for each of the components, specifications for system pressures, temperatures and fluid, and preliminary designs for each component. Detail design of the components then proceeded on separate but related projects. During the detail design and development of the individual components, the original specifications were modified slightly to reflect compromises or new information attained during the development process. The overall cycle performance objectives did not change.

The thermodynamic cycle and state points for the baseline reverse Brayton cycle are shown in Figure 2.1. The compressor, at the warm end of the cycle, forces the gas to flow through the cycle as a result of the pressure ratio through the machine. The gas expands through the turbine, at the cold end, producing refrigeration. This refrigeration is available to cool the load and to compensate for losses in the heat exchanger and for parasitic heat leak from the surroundings. The heat exchanger transfers heat from the warm, high pressure gas to the low pressure stream returning to the compressor. The flow of gas is continuous.

There are two performance characteristics of the heat exchanger which are critical: thermal effectiveness and pressure loss. The thermal effectiveness is a measure of the required difference in temperature between the streams to transfer the heat from the incoming flow. The pressure drop is a measure of the penalty to the cycle as a result of this transfer of heat. The effects of reduced performance can be summarized by considering the effects at the cold end.

Pressure losses through the heat exchanger reduce the available pressure ratio for expansion through the turbine. For an ideal gas, the net refrigeration available from the turbine is:

$$q_t = \eta\, m\, c_p\, T_{in}\, (\pi^{(k-1)/k} - 1) / \pi^{(k-1)/k}$$

where η is the overall turbine efficiency, m is mass flow rate, c_p is the specific heat, T_{in} is the temperature at the inlet to the turbine, k is the ratio of specific heats and π is the pressure ratio at the turbine. In Figure 2.2, the solid curves show how pressure losses affect the turbine output for a fixed flow rate and range of pressure ratios. The Figure shows that the penalty for

Creare

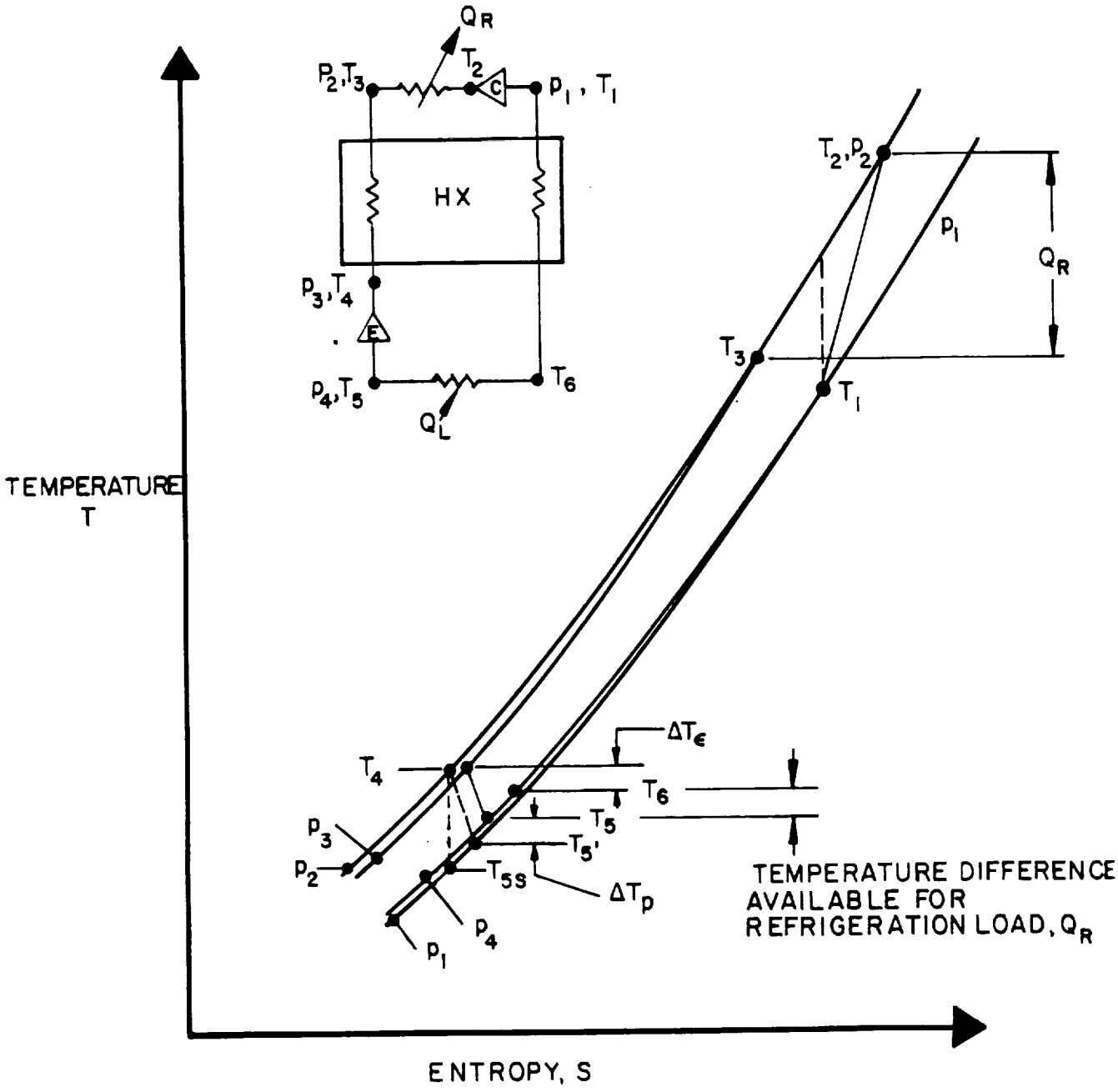

Figure 2.1 THERMODYNAMIC CYCLE

Creare

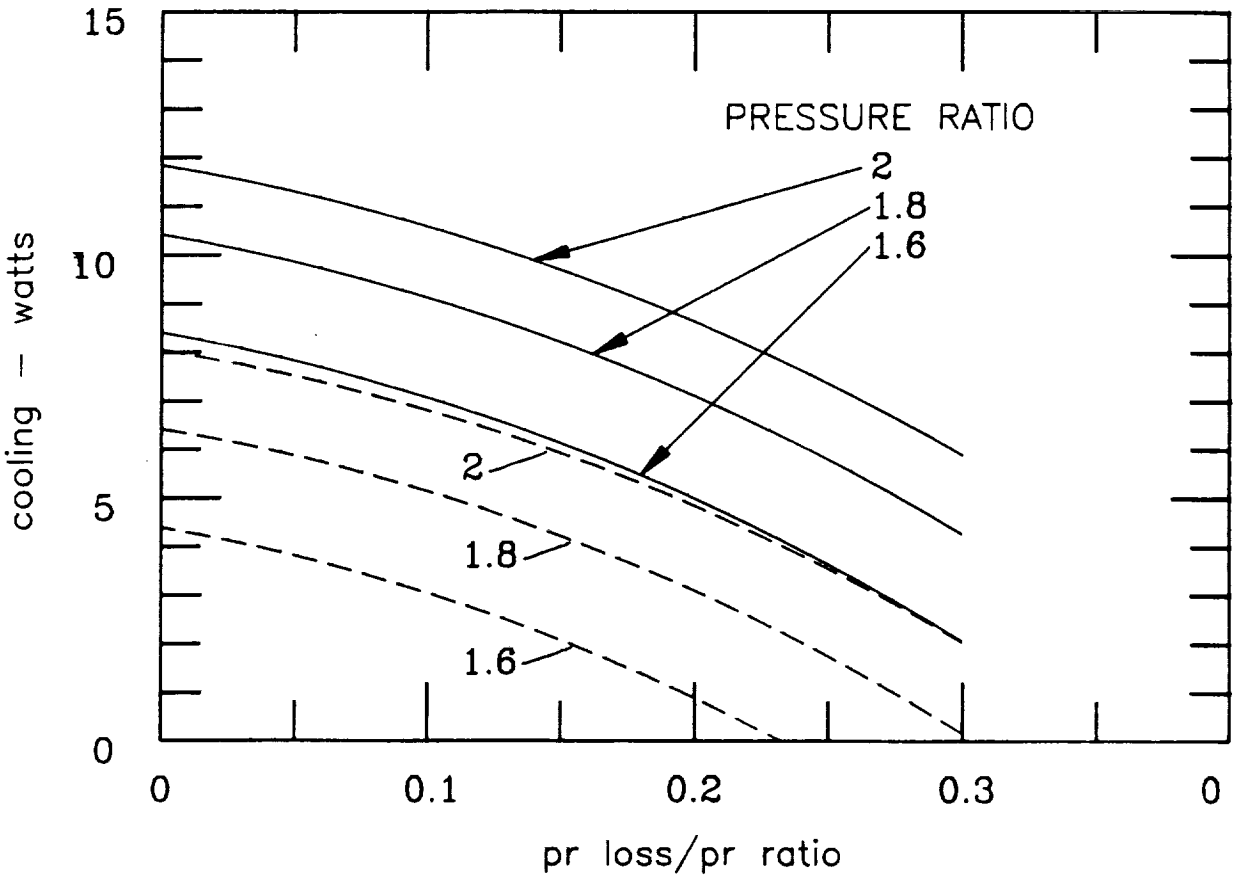

Figure 2.2 EFFECTS OF PRESSURE LOSSES ON CYCLE COOLING CAPACITY.
SOLID CURVES = TURBINE OUTPUT, DASHED CURVES = CYCLE CAPACITY

Creare

increased pressure losses is significant in terms of reduced refrigeration. For the 5 W baseline cycle, about 4 watts of the refrigeration from the turbine is required to offset the ineffectiveness of the heat exchanger (assuming a nominal thermal effectiveness of 0.985). Therefore, this value must be subtracted from the turbine output to assess the effect of pressure loss on refrigeration capacity available from the cycle. The dashed curves show this relationship.

The design target for pressure loss was arrived at by a more complicated modelling process - one which incorporated all important loss mechanisms (see Section 5.). The result was pressure losses of 2.6 kPa in the high pressure stream and 1.5 kPa in the low pressure stream. For a nominal cycle pressure ratio of 1.7, these combined pressure losses give a pressure loss to pressure ratio of 0.024.

The thermal effectiveness for the heat exchanger is a measure of the ΔT between streams required to produce the required heat transfer. High thermal effectiveness is critical to the overall cycle performance because the losses which lower the effectiveness usurp useful refrigeration from the turbine. A more useful way of characterizing the thermal behavior of the heat exchanger is through the ineffectiveness, the ratio of the ΔT between gas streams at the cold end, to the ΔT between the warm and cold end. The turbine produces a temperature drop as a result of expanding from high pressure to low pressure. This temperature difference is then used to absorb heat from the load and to provide the ΔT potential required in the heat exchanger.

An example of the leverage of effectiveness on cycle performance is the comparison between the design target of 0.985 and the expected effectiveness as a result of testing. For the baseline cycle, a thermal effectiveness of 0.985 results in 4 W of turbine capacity required for the heat exchanger, and 5 W for the load. If the thermal effectiveness is increased to 0.992, the refrigeration requirement to compensate for losses in the heat exchanger is reduced to 2.2 W which increases the net refrigeration capacity of the cycle from 5 W to 6.8 W. The effect is to raise the cycle capacity by 36% without changing input power requirements.

Virtually all features of the design were focused on maximizing performance within tolerable mechanical and fabrication constraints. Some of the constraints were rigorous. An example is that no organic materials would be allowed in the final assembly. Others were established through key experiments during the design. These included issues such as the minimum slot width which could be produced with acceptable uniformity and within acceptable time. The final product of the scoping studies and trades was a set of specifications, which included performance targets from which detailed design and fabrication exercises were performed. These specifications are given in Table 2.1.

The specification for launch was not rigidly characterized. The structural integrity of the heat exchanger during launch will depend significantly on the transmissibility of the support structure. Our approach was to design the assembly so that it was as mechanically robust as was feasible under the constraints of time and budget for this project, and to identify methods for providing additional support when it is finally interfaced to the rest of the cryocooler assembly.

Creare

Table 2.1 Heat Exchanger Specifications	
Performance	
Fluid	
Neon	
Flow Rate	1.3 g/s
Inlet Temperature (High press. side)	260 K (+40/-0°C)
Inlet Temperature (Low press. side)	70 K (+5/-5°C)
Inlet Pressure (High press. side)	170 kPa (± 30 kPa)
Inlet Pressure (Low press. side)	100 kPa (± 20 kPa)
Maximum Internal Pressure	400 kPa
Thermal Effectiveness	> 0.985
Pressure Loss (High pressure side)	2.6 kPa
Pressure Loss (Low pressure side)	1.5 kPa
Mechanical	
Mass (core)	< 5 kg
Length	< 0.5 m
Outside Diameter	< 0.1 m
Other	• All metal construction • Withstand Launch Environment • Non Contaminating for Long Life Cryo Environment

3. HEAT EXCHANGER DESIGN

The heat exchanger is a counter flow recuperator in which high pressure gas flows through a central tube, giving up heat to the flow of low pressure gas through an annular tube which surrounds the central tube. Figure 3.1 is a cross section of the heat exchanger assembly. There are 300 copper disks axially positioned along the length of the center tube. Each disk is perforated with two annular rows of slots. Three hundred copper rings are located at matched axial positions along the length of the annular space. The copper rings also have two annular rows of slots cut through. Figure 3.2 is a photograph of a disk/ring pair with slots. The tubes are redrawn 321 stainless steel, with a nominal wall thickness of 0.13 mm (0.005"). The outer tube is 87 mm (3.4") diameter and the inner tube diameter is 68 mm (2.7").

Each copper disk and copper annular ring contains slots which are arranged in concentric circles. The number and size of slots in each disk or ring can be adjusted and controlled to account for changes in density through the heat exchanger. The manipulation of slot width and number can also aid in control of flow maldistribution. In this design, the selection of size and quantity of slots was a compromise between fabrication challenges, thermal performance and pressure loss. Table 3.1 summarizes the important dimensional characteristics of the disks and rings. Each of the disks and rings was slightly dished to provide some rigidity against deformation during assembly.

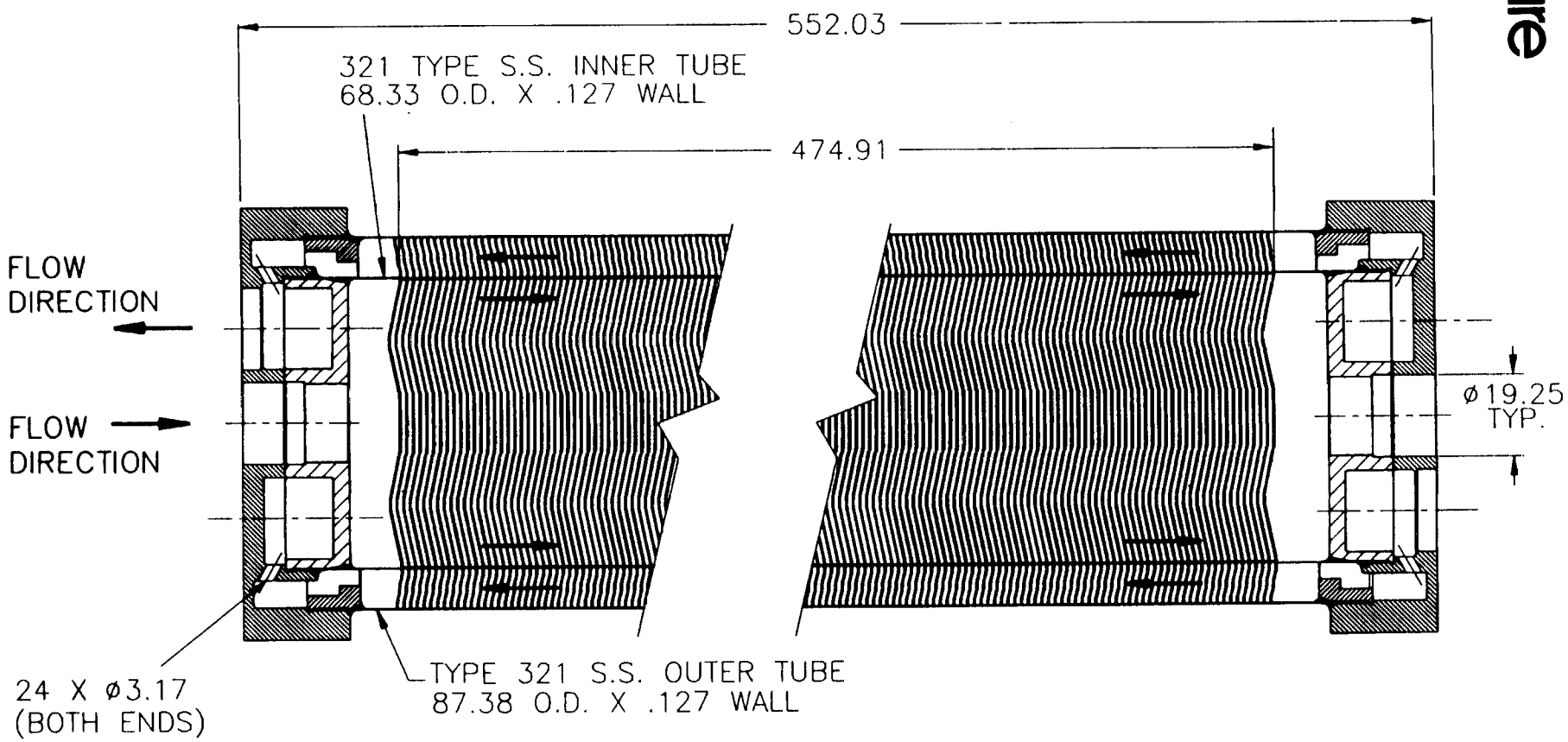

Figure 3.1 ASSEMBLY OF THE HEAT EXCHANGER
All dimensions in millimeters

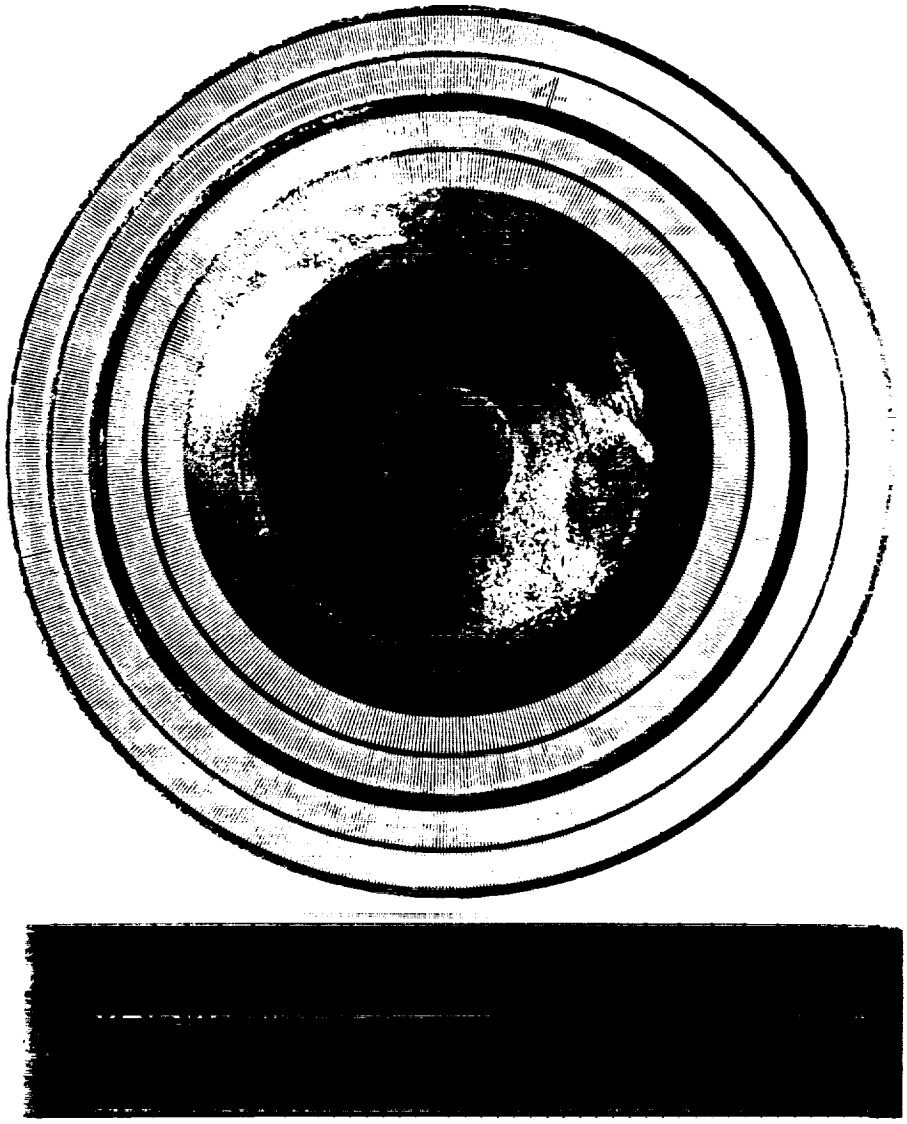

Figure 3.2 INNER DISK AND ANNULAR RING WITH SLOTS

Creare

Table 3.1 HEAT EXCHANGER SLOT DISTRIBUTION		
	Disks	Rings
Total Number	300	300
Thickness	0.4 mm	0.4 mm
Slot Width	0.11 mm	0.16 mm
Slot Length	3.56 mm	3.56 mm
# Slots (inner array)	592	691
# Slots (outer array)	691	769
Material	C10200	C10200

Each pair of matching disks and rings is located to within 20 μ axial distance of each other. The disk and ring are soldered to the central tube using a controlled process. The resulting joint must be mechanically robust. However, the thermal conduction quality of the joint is most important. The fillet on each side of the joint must be large enough to provide good radial conduction, but small enough to inhibit significant axial conduction. This was achieved using a nominal solder thickness of 20 μ coated on each tube surface. There is no solder joint between the rings and outer tube. Mechanical support for the tube is provided at the end caps, and there is no need for thermal contact between the outer tube and rings.

The nominal gap between the outer tube and the outside diameter of the rings is 25 μ. The differential thermal contraction between the copper and stainless is approximately 0.03% over the temperature range 300 K to 60 K. This implies an increase in gap of about 25 μ (or a doubling of the gap at the cold end. The ideal gap would be 75 μ which would further enhance heat transfer between the gas and copper rings. Performance would begin to deteriorate if the gap became grater than about 150 μ.

The initial design of the heat exchanger anticipated the use of interference fits between the disks, central tube and rings during assembly to hold the relative position of each disk/ring pair until soldering. Fabrication trials showed this to be impractical. A series of indentations (dimples) were located in the wall of the central tube during the assembly process to positively lock the disks in place for soldering (see Section 4 for additional discussion). For the initial assembly, the rings were carefully positioned by eye to within 25 μ of the edge of existing dimples. A slight interference fit between the rings and the tube held them in position until soldering.

The end caps (headers) are stainless steel. They provide for low pressure loss distribution of the flow between the external ports and the internal central and annular flow passages. They are soldered subassemblies which provide structural restraint for the tubes which are soldered to them.

4. FABRICATION ISSUES

Several challenging fabrication issues were dealt with in the project. The most important of these are listed below and discussed in this section.

Greare

- Precision machining of slots. A large quantity of small slots had to be machined into many disks with precision - both in terms of location and slot geometry. A semi automated facility was used for electric discharge machining of the slots.

- Tube fabrication. Initially thought to require development of special tooling, a supplier of acceptable drawn tubing was located.

- Fastening. Joints between disks, the central tube and rings required careful design and development. The solder joints must be robust, provide for good radial conduction and limited axial conduction.

- Assembly and positioning. The assembly and fixturing of 300 pairs of disks and rings with accuracy required the development of special tooling.

An element which was critical to achieving the performance targets within the size constraints was the ability to machine the slots in the disks and rings with the required level of precision. In order to do so, a semiautomatic facility with specially developed electric discharge machining techniques was used.

The facility consists of eight stations. In each station, a single disk or ring was machined. All stations could operate simultaneously. Each station consisted of an electric discharge center and a controlled circular table which was rotated (indexed) to precise angular positions. The number of positions was programmed in a numerical controller, indexing performed by stepping motor and gearing. Once the table location was set, the electric discharge machining device was activated and a slot was cut in a single disk or ring - if other stations were also operating, other slots were also cut simultaneously. The electric discharge machining system consisted of circuitry to tailor the voltage and spark duration and frequency for surface finish and speed, a drive mechanism to advance the electrode, and the electrode which was a continuous reel of molybdenum ribbon. Figure 4.1 is a photograph of the machine during assembly. Seven rotary tables and two ribbon systems are illustrated.

The machine is capable of a metal removal rate in excess of 0.5 mm^3/min at a single station. Slots as narrow as 70 μ can be machined in metal plates in excess of 800 μ in thickness. Once set up, eight elements were machined, unattended in a period of about 22 hours. The machined elements were manually removed, cleaned and inspected, and new blanks installed for the next run. The quality of the slots was high. Slot to slot width variations were within 5 μ (0.0002"), and the variation in slot width in a given slot was less than 5 μ. In general, the slots were tapered by this amount.

The sequence for assembling the heat exchanger consists of the following steps:

1) Machining of disks and rings, coating of disks and rings, machining of end caps, machining and tinning of the central tube, and machining of the outer tube. All approximately parallel operations.

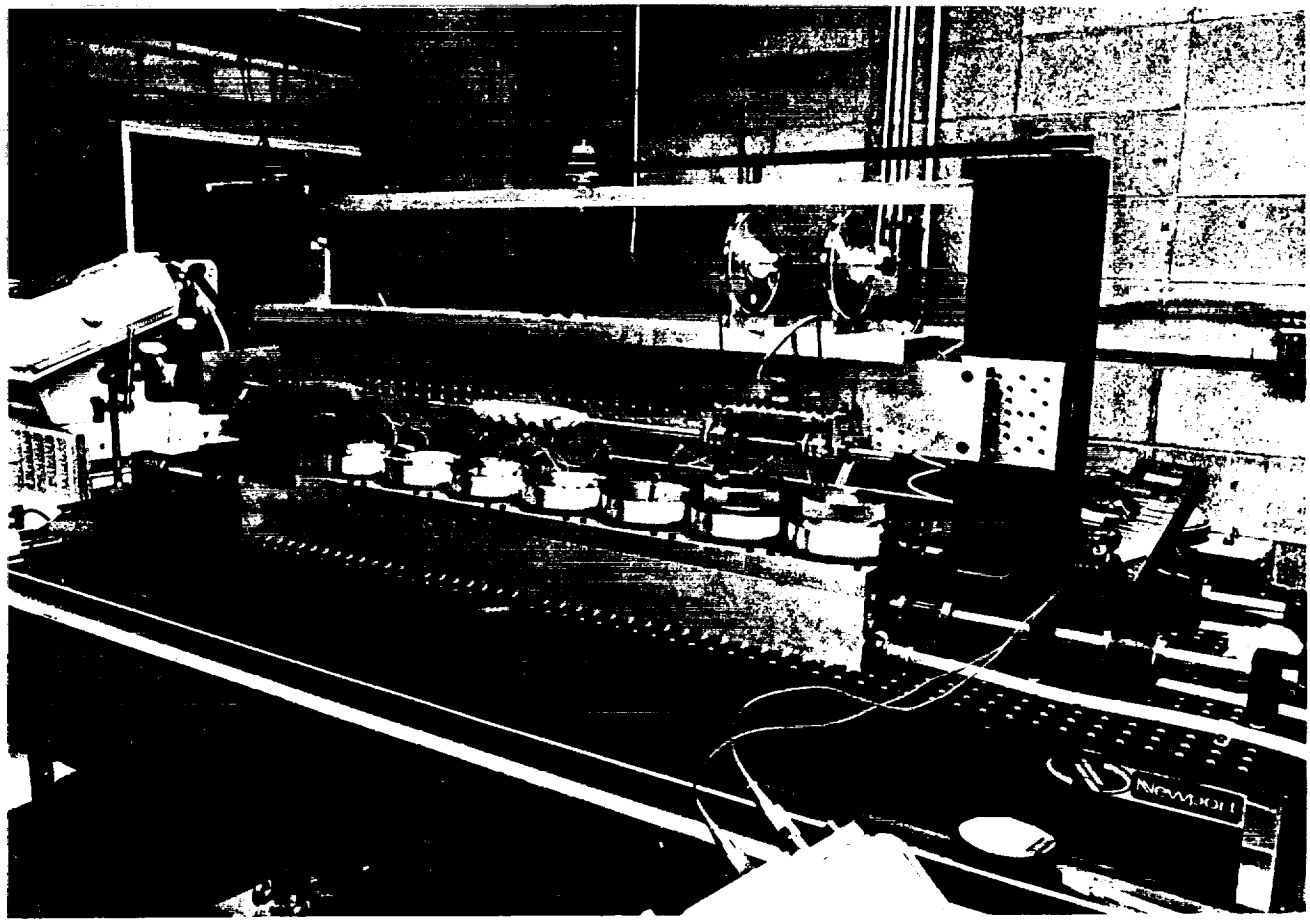

Figure 4.1 PARTIALLY ASSEMBLED SLOT CUTTING MACHINE

2) The disks and rings are then assembled into and onto the central tube, using dimples to locate each disk/ring pair.

3) The core assembly is mechanically joined using a freon reflow soldering process in a high temperature vapor bath.

4) The core and outer tube are soldered to one end cap, then the other using thermal sinks to prevent overheating of the previously soldered assembly.

The critical elements within the fastening and joining operations involved developing and selecting suitable materials and processes for tinning, flux soldering, and cleaning. Many empirical tests were performed on mock ups and subassemblies to define the "best" methods and materials. The final test article assembly embodies the methods which were judged to give the highest quality result in these areas.

Some mechanical tests were performed. The most notable test involved a hydrostatic pressure test to evaluate the integrity of the outer tube and solder connection with the end cap. Figure 4.2 is a photograph of the outer "cylinder" pressurized to 3 Mpa - approximately 7.5 times the maximum expected operating pressure. It was at this pressure that a solder joint failed with a small quantity of leakage detected.

5. THERMAL DESIGN

The model used to predict the thermal performance of the slotted plate heat exchanger was developed in Phase I and is documented in the Phase I Final Report [1]. The tests performed in Phase II indicated that the original model was overly conservative and that actual losses in the heat exchanger are substantially lower than anticipated. The early models were revised to remove some of the conservatism and excellent agreement with the experimental results was obtained. In this section we summarize the approach used in the original model and describe in detail the modifications to those models.

The six mechanisms contributing to the losses in the heat exchanger are:

1. convective resistance between gas and the copper plates,
2. conduction resistance in the copper plates and the stainless tube separating the low and high pressure streams,
3. axial conduction along both stainless steel tubes,
4. axial conduction in the copper plates themselves, and
5. pressure drop.

The first four mechanisms result in a measurable temperature difference between the cold and warm streams of the heat exchanger. The last mechanism, pressure drop, reduces the temperature drop in the expansion device and thereby decreases the cooling capacity of the cycle. As discussed in the Phase I Final Report, the losses associated with the pressure drop can be included in the overall performance of the heat exchanger as an additional temperature drop. This simplifies the optimization of the heat exchanger geometry to minimize the combined thermal and pressure losses.

Creare

ORIGINAL PAGE
BLACK AND WHITE PHOTOGRAPH

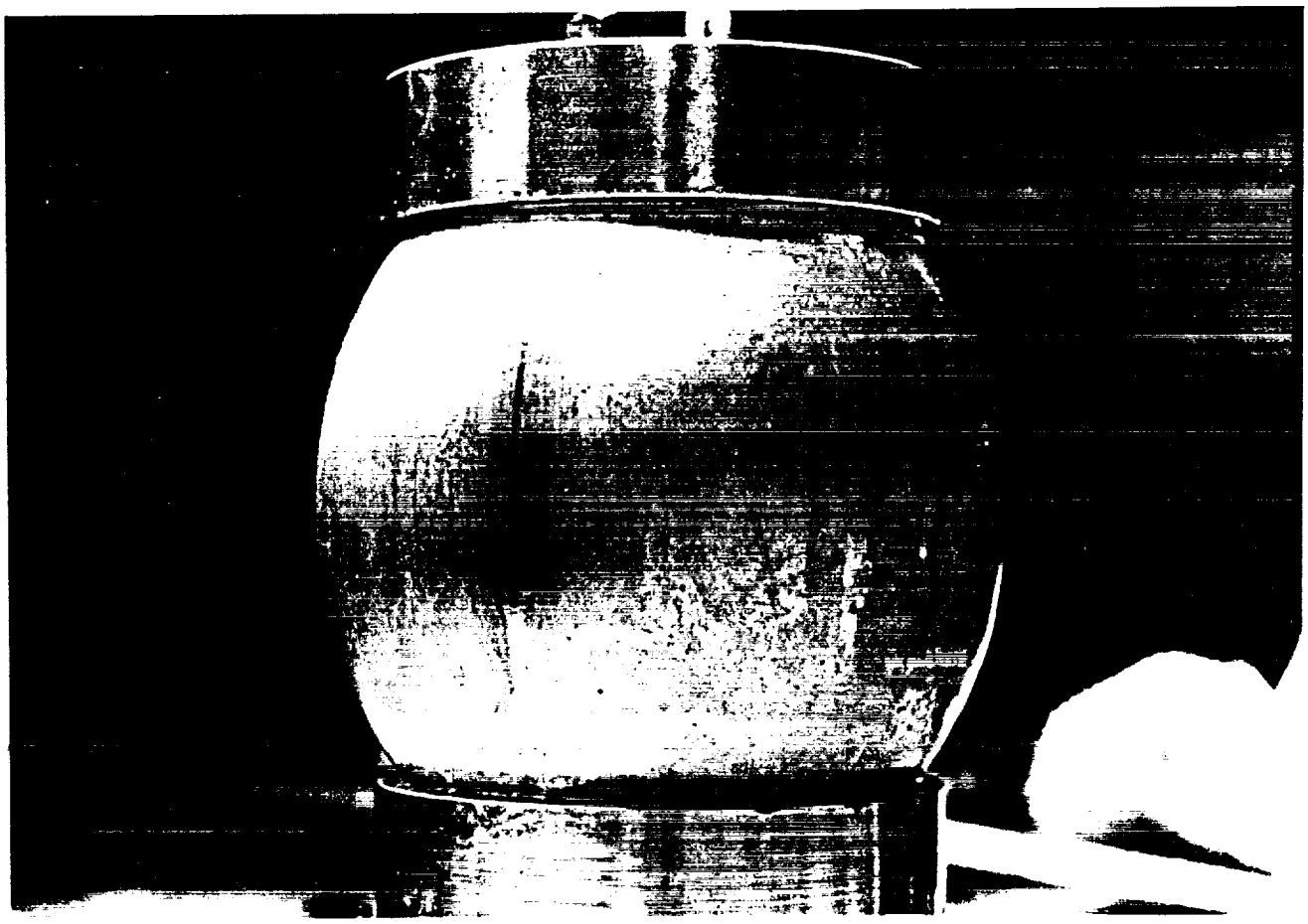

Figure 4.2 PRESSURE TEST OF OUTER CYLINDER AND SOLDER JOINTS

Creare

In the original model each loss mechanism was assumed to act independently of the others, and the temperature drop associated with each one of them were simply added to obtain the overall temperature difference across the streams of the heat exchanger. This approach is conservative because, as explained below, the losses associated with convection of the gas stream and conduction in the copper plates are highly coupled. Only in the case of infinite heat transfer coefficient (zero convection losses) are the two loss mechanisms additive. In all practical applications, the combined loss is substantially lower than the sum of the two separate losses.

Figure 5.1 a and b illustrate the Phase I model for the convective and copper axial conduction losses. The figures show the assumed gas and solid temperature profiles across any given plate for the two limiting situations of no axial conduction in the copper (Figure 5.1a) and no gas convection losses (Figure 5.1b). If the copper axial conduction losses were not present, the temperature difference attributed to gas convection losses would be given by the familiar expression for a balanced, counterflow heat exchanger [Kay's & Landon]

$$\Delta T_f = \frac{1}{1 + NTU} \tag{1}$$

where the Number of Transfer Units (NTU) is defined as:

$$NTU = \frac{Ah}{2\ \dot{m}\ c_p} \tag{2}$$

A ≡ total slot heat transfer area
h ≡ gas heat transfer coefficient
$\dot{m}$ ≡ gas mass flow
c_p ≡ gas specific heat

Even if the NTU were infinite, the temperature difference between the two gas streams in the heat exchanger would not be zero because of the effect of axial conduction in the copper plates. For example, in a heat exchanger with 1 plate, the two gas exit temperatures are at best equal to each other (and equal to the temperature of the copper plate). Axial conduction in the copper plates effectively changes each plate into a parallel flow heat exchanger rather than a counterflow heat exchanger. In the limit, when the NTU becomes very large, the temperature difference between the two gas stream approaches:

$$\Delta T_n = \frac{1}{N + 1} \tag{3}$$

In the Phase I model we simply added (1) and (3) in calculating the total losses.

Equations (1) and (3) represent the upper bounds for the convection and copper axial conduction losses, for the limiting situations in which one of the loss mechanisms is negligible compared to the other one. We have found that for designs with very high overall effectiveness, the simple addition of these two upper bound estimates substantially overpredicts the magnitude of the combined losses. Figure 5.1c. illustrates the actual temperature profiles across any given plate in the heat exchanger. Because of the high thermal conductivity of the

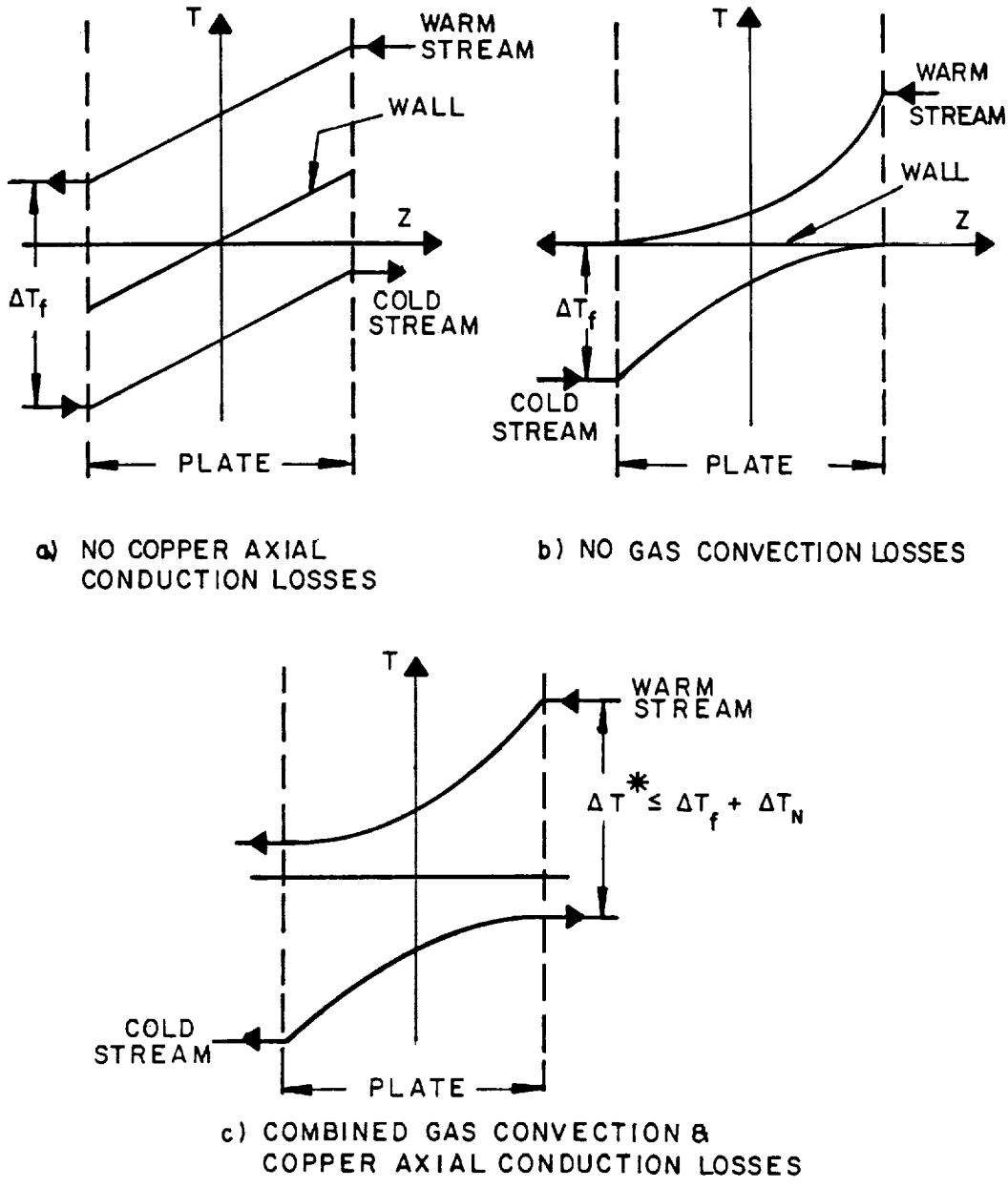

Figure 5.1 GAS CONVECTION AND COPPER AXIAL CONDUCTION LOSSES

Creare

copper plate, its temperature is uniform. The two gas streams exchange heat with this constant temperature plate and, hence, their temperature profiles have the characteristic exponential variation with distance into the slots. After some straightforward, but lengthy algebra, one can obtain the combined loss as:

$$\frac{\Delta T^*}{\Delta T_{max}} = \frac{1}{1 + \frac{N\,(1 - e^{-2\,NTU/N})}{(1 + e^{-2\,NTU/N})}} \qquad (4)$$

Figure 5.2 compares the sum of the two bounding losses (Phase I model) with the combined losses predicted by Eqn (4). It can be seen that for the design conditions of NTU = 291 and N = 300, the Phase I model overpredicts the combined losses by 60%.

A second correction which was implemented in the heat exchanger model is related to the calculation of the losses associated with axial conduction in the stainless steel tubes. In Phase I it was assumed that both tubes are in intimate thermal contact with the plates. Therefore, the effective conduction length for both tubes was equal to the sum of the spaces between the plates. In practice, the outer tube is not bonded to the rings and there is a small gap between the rings and the tube. The effective conduction length for the outer tube is therefore equal to the full length of the heat exchanger. Although the change in conduction length is on by about 30% for the full size heat exchanger, it is a much larger (factor of 3) for the subscale test article. The Phase I model, therefore, significantly overpredicted the stainless steel tube axial conduction losses.

As discussed in Section 6, the experimental results obtained with the subscale test article are well predicted by the revised models. We anticipate that the overall effectiveness of the full size heat exchanger will be 0.99 rather than the 0.985 target. This represents a 30% reduction in heat exchanger losses.

6. TESTING

A test article was fabricated to obtain performance data which could be used to check the thermal model predictions. The test article consisted of 14 pairs of plates and disks fabricated and assembled in the same manner as would be used to build an entire heat exchanger. Performance tests were performed in air over a broad range of flow rates at several internal pressures. The tests were designed to yield data for flow rates which bracket the design point.

Thermal effectiveness was calculated from temperature measurements. Flow was measured using a rotameter, and a small heater in the gas flow path provided some redundancy to flow and temperature measurements by means of an energy balance. Pressure losses in the high and low pressure passages in the heat exchanger were also measured and compared with predictions. The measurements were made in the core alone and for the overall assembly including headers. The results of the tests indicated that certain simplifying assumptions in the original model had to be modified - the test results gave significantly higher performance than predicted. After upgrading the model, test results and predictions correlate very well.

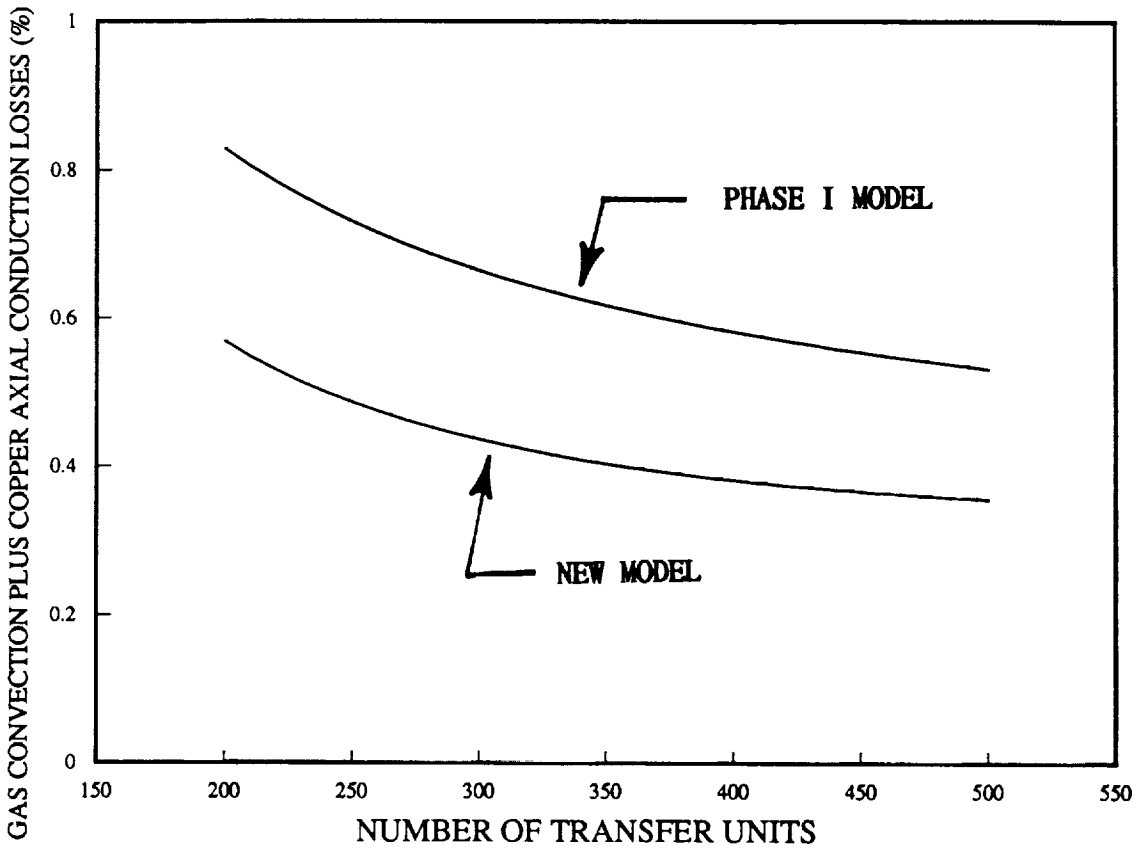

Figure 5.2 GAS CONVECTION AND COPPER AXIAL LOSSES

Creare

This section describes the test article, tests performed, instruments and measurements, and methods of reduction of data. Results are presented and compared with predictions, and the implication of the test results on the predicted performance of the heat exchanger are discussed.

6.1 Test Article

The test article consisted of an assembly of 14 pairs of copper disks and plates in their respective stainless steel tubes. The ends of the tube assembly were capped with soldered headers. Figure 6.1 is a cross section drawing of the test article. The disks and plates are prototypical of the heat exchanger design, as are the tubes and methods of fabrication and assembly. The test article represented the first successful demonstration of all the necessary fabrication methods.

The tests were performed with air at nominal room temperature. Instead of trying to provide cooling (as would occur in a cryogenic refrigerator), one end of the heat exchanger was supplied with room temperature air, the exit stream at the other end was heated. A valve at the warm end of the heat exchanger provided a pressure drop so that the two streams could be adjusted to close to prototypical values.

Figure 6.2 is a drawing of the test arrangement. The test article was supported in space on the inlet and exit tubes at the cold end of the assembly. The heating element and valve are shown at the upper (warm) end of the unit. A vacuum vessel was used to provide convective and conductive isolation from the atmosphere. Appropriate electrical and plumbing vacuum feedthroughs were located in the baseplate. Multilayer insulation was wrapped around the entire test article assembly to reduce radiation from the walls of the vacuum vessel to the test assembly. Figure 6.3 is a photograph of the test article prior to multilayer wrapping. The wrapped assembly is shown in Figure 6.4, and the test set up with the vacuum vessel is shown in Figure 6.5.

6.2 Measurements and Instrumentation

For each set of test conditions, temperatures, pressures and flow rate were recorded. These data were sufficient to completely characterize the performance of the test article over a range of flow rates. Figure 6.6 is a schematic identifying the important instruments and measurement locations.

Temperatures were measured by means of calibrated glass bead thermistors which were encapsulated in insulating PVC (Figure 6.7) to provide robustness to the leads and low thermal conductivity to external supports. The thermistors were inserted into the gas path at each location by epoxying the encapsulation into a hole into the tubes. In general, the thermistors extended approximately 1 cm into the tube. Resistance changes for the thermistors were read on a Hewlett Packard digital multimeter.

Pressures were measured using bourdon gages and Magnehelic differential gages. The Magnehelic differential gages were used to establish the pressure losses in the direction of flow where very low ΔP's were expected. The static gages were used to establish internal static pressures.

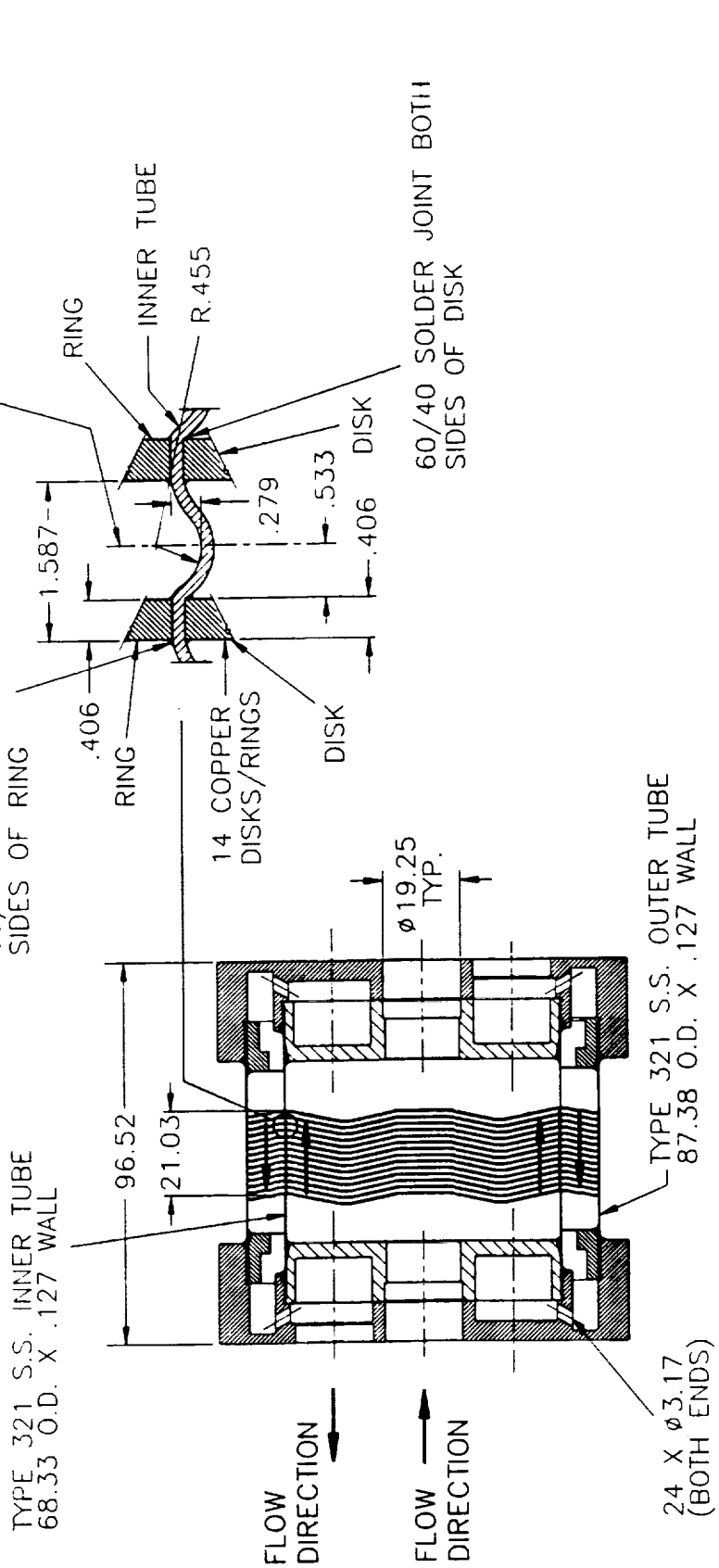

Figure 6.1 CROSS SECTION OF TEST ARTICLE
All dimensions in millimeters

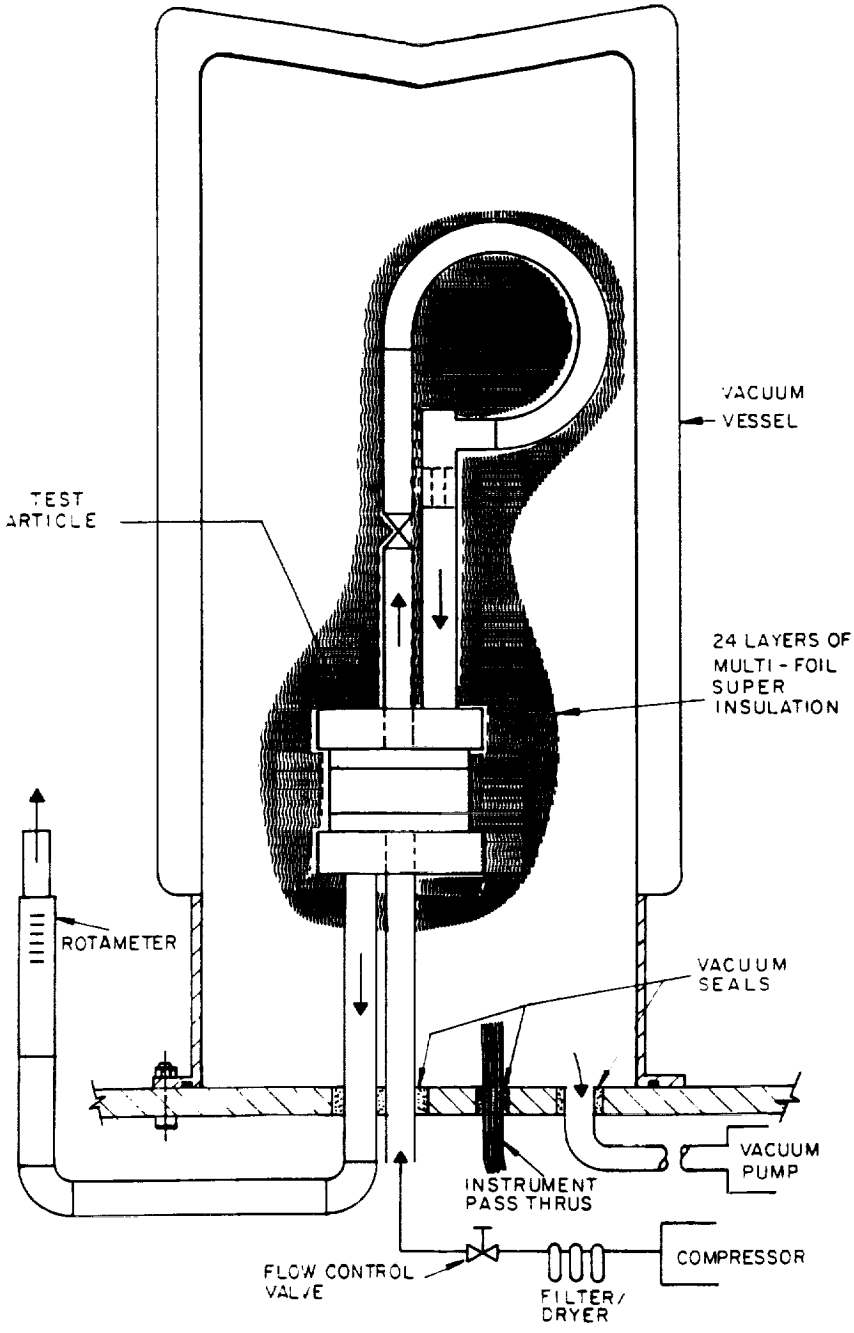

Figure 6.2 TEST ARRANGEMENT

Creare

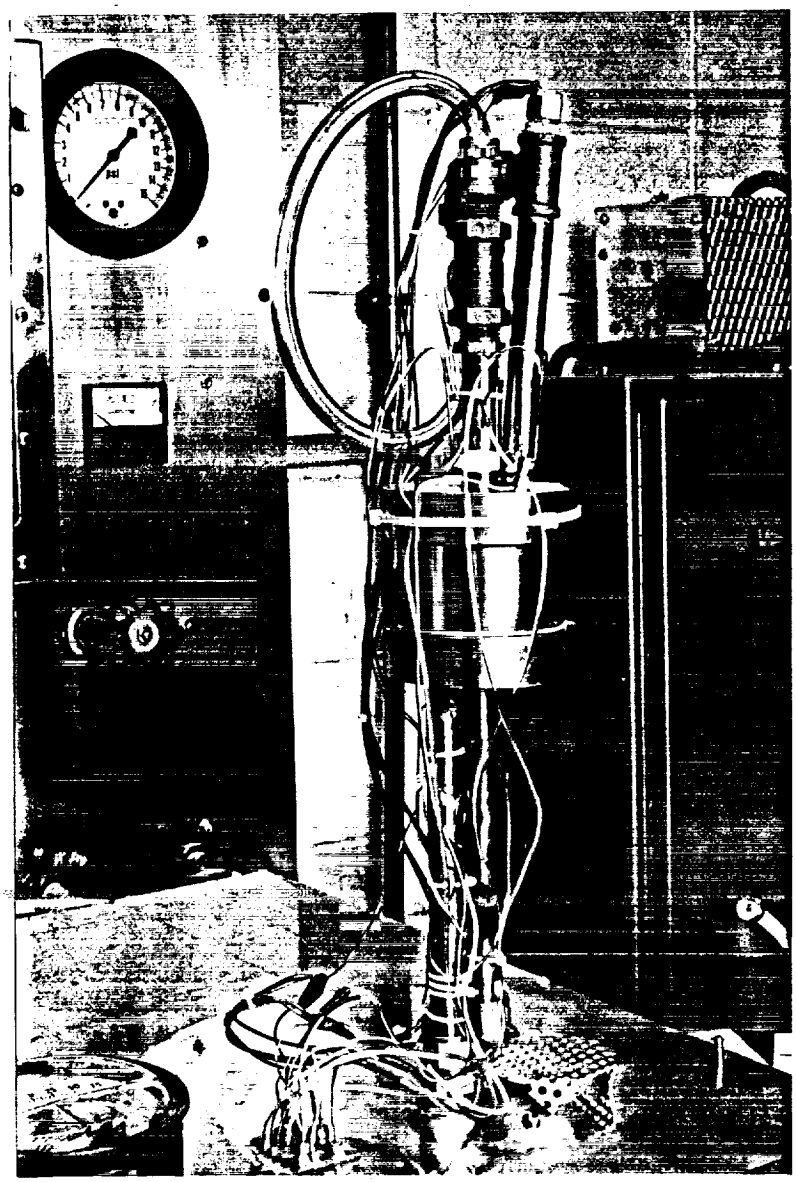

Figure 6.3 TEST ARTICLE PRIOR TO INSULATION

Creare

ORIGINAL PAGE
BLACK AND WHITE PHOTOGRAPH

Figure 6.4 TEST ARTICLE AFTER MULTILAYER INSULATION

Creare

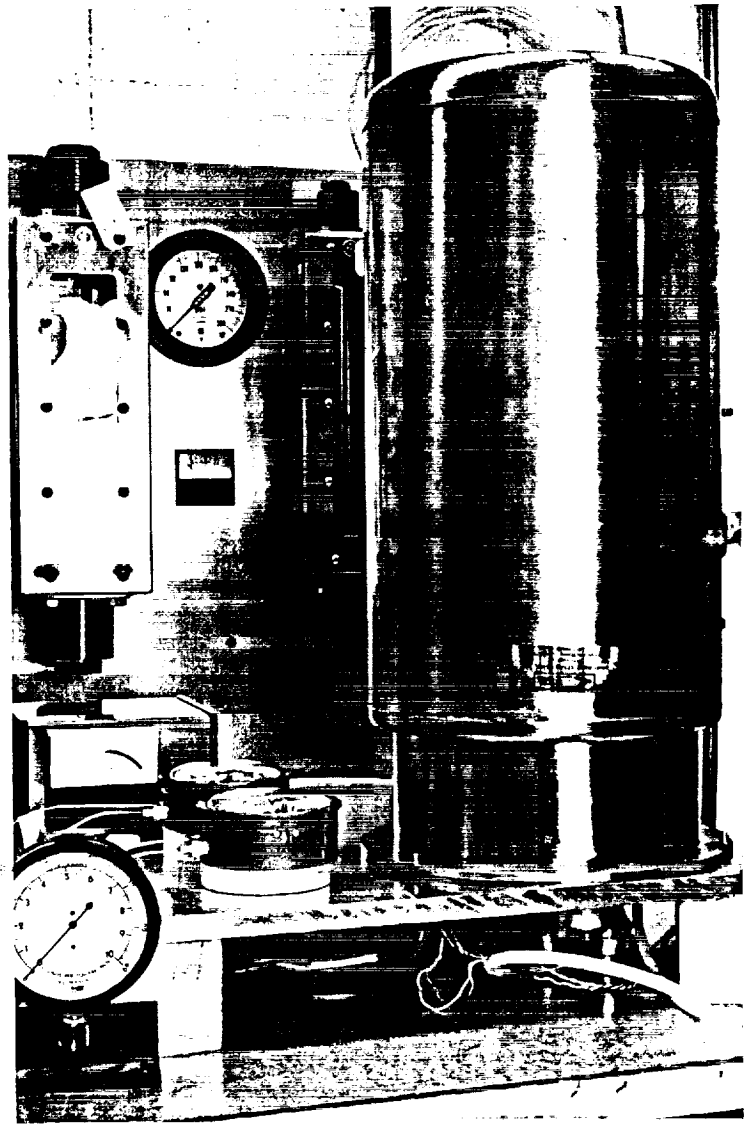

Figure 6.5 TEST ARRANGEMENT IN VACUUM VESSEL

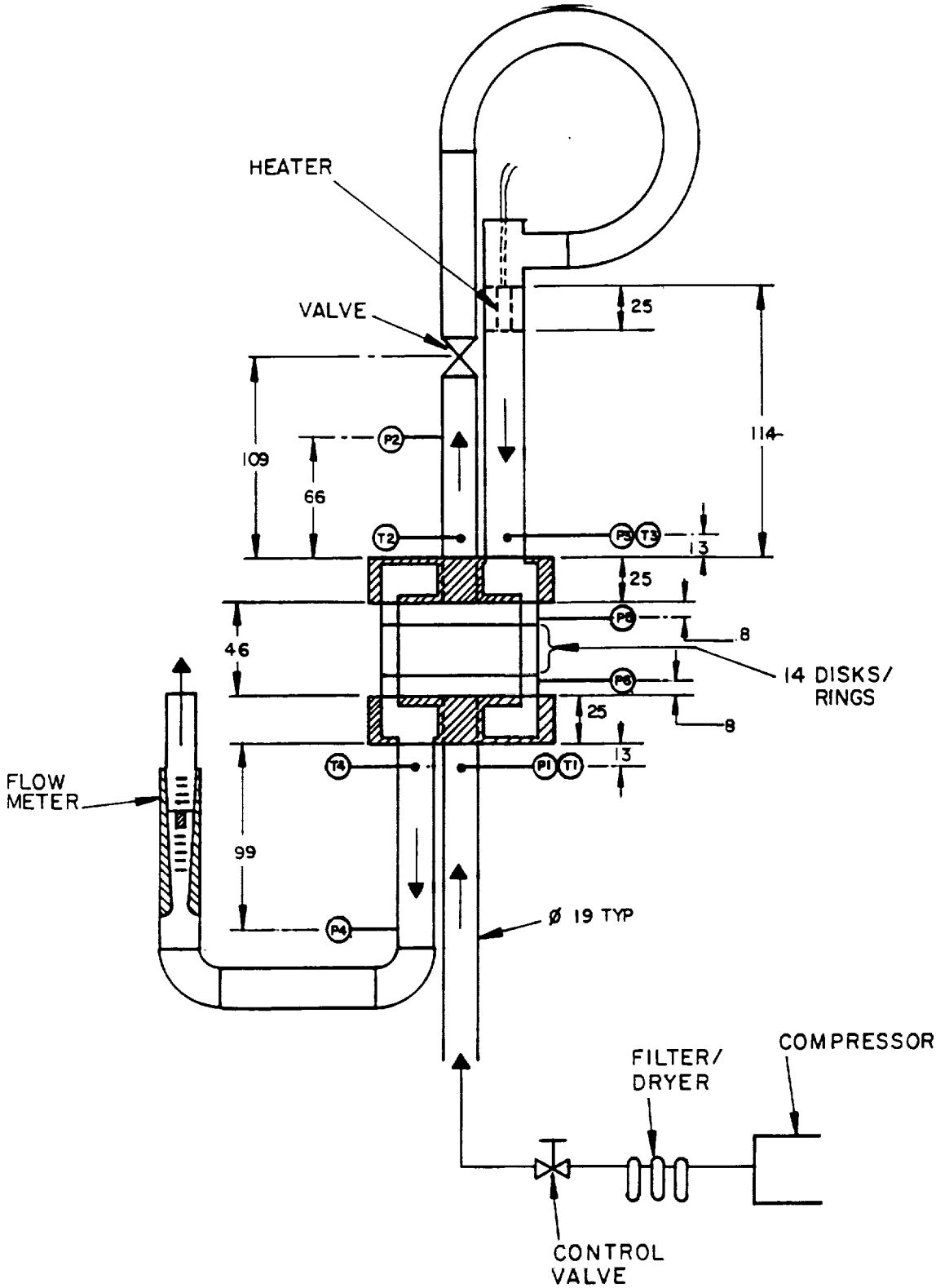

Figure 6.6 INSTRUMENTS FOR PERFORMANCE TESTING
All dimensions in millimeters

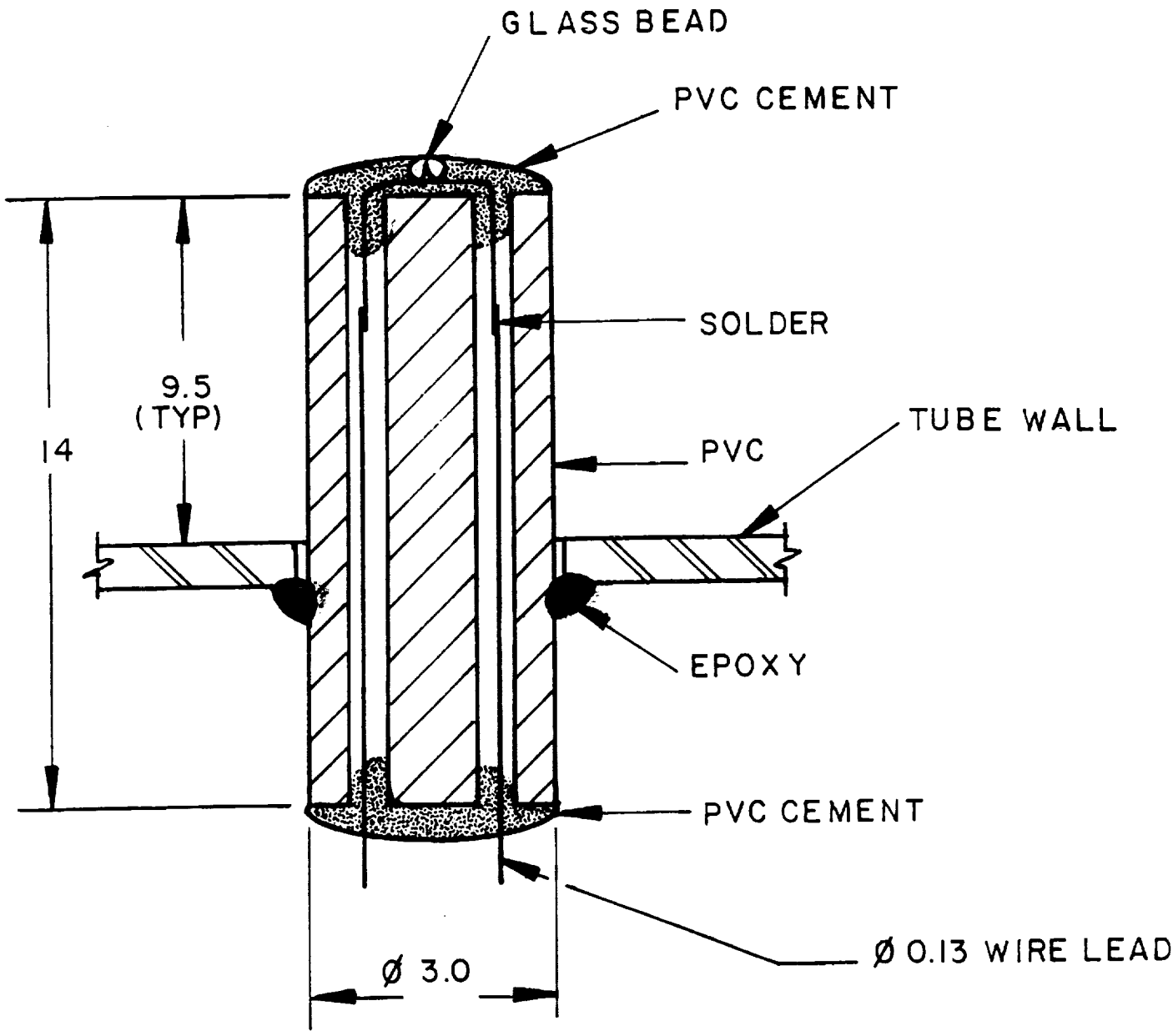

Figure 6.7 THERMISTOR ENCAPSULATION AND MOUNTING DETAIL
All dimensions in millimeters

Creare

Flow rate was monitored using a single calibrated rotameter for low flow testing and two rotameters in parallel for very high flow rates.

Temperature differences at the warm end were generated with a small resistance heater element inserted in the gas stream downstream from the pressure drop valve. The heater was nominally limited to about 2.6 watts in order to stay within the calibrated temperature limits on the thermistors. DC voltage across the 10 ohm resistance was monitored using an HP digital multimeter. A consistency check between measured flow rate, T2, T3 and heater input power showed that uncertainties were very low.

6.3 Performance Tests

Dried and filtered air was supplied from a compressor through a flow control valve to the inlet (high pressure) port of the test article. Pressures and temperatures are measured at locations identified in Figure 6.6. Flow rate was monitored at the exit of the cold end discharge line. During some tests at high mass flow rate, the exit line from the rotameter was regulated to elevated pressures to raise the air density. In general, the time constant for test conditions to stabilize was very long. After initial settings, conditions were monitored until changes in temperature were less than 0.1°C in ten minutes prior to recording data. This settling period was generally about 3 hours for a test condition.

Three series of tests were run. In the first, flow rates were restricted to near 1 g/sec. These test were intended to give performance very close to the design point. Pressure losses and thermal performance were measured concurrently. The exit pressure from the test article was atmospheric. After the initial series, a broader range of flow conditions was sought. In order to attain higher flow rates, the discharge from the rotameter was regulated to higher pressures to increase air density. Thermal performance was measured at these elevated pressures. In order to measure pressure losses at high flows, a third series of tests were run at a nominal atmospheric discharge pressure, but without temperature measurements. Only pressures and flow were recorded.

6.4 Results

Figure 6.8 and 6.9 show the test results in comparison with calculated predictions using the original and upgraded thermal model.

The thermal performance of the test article is summarized in Figure 6.8. The figure shows the variation in thermal effectiveness with mass flow rate. The data are plotted in terms of 1 - ε where thermal effectiveness ε is calculated from:

$$\varepsilon = (T_3 - T_4) / (T_3 - T_1)$$
$$1 - \epsilon = (T_4 - T_1) / (T_3 - T_1)$$

The figure also shows a comparison between performance predictions and results of the tests.

The two curves present predicted thermal performance of the test article in air for a range of flow rates up to 3 g/s. The curve labelled "original model" gives predictions based on the original modelling approach used to design the heat exchanger. The "upgraded model" curve incorporates modifications to some of simplifying assumptions incorporated in the original model (see Section 5. for discussion).

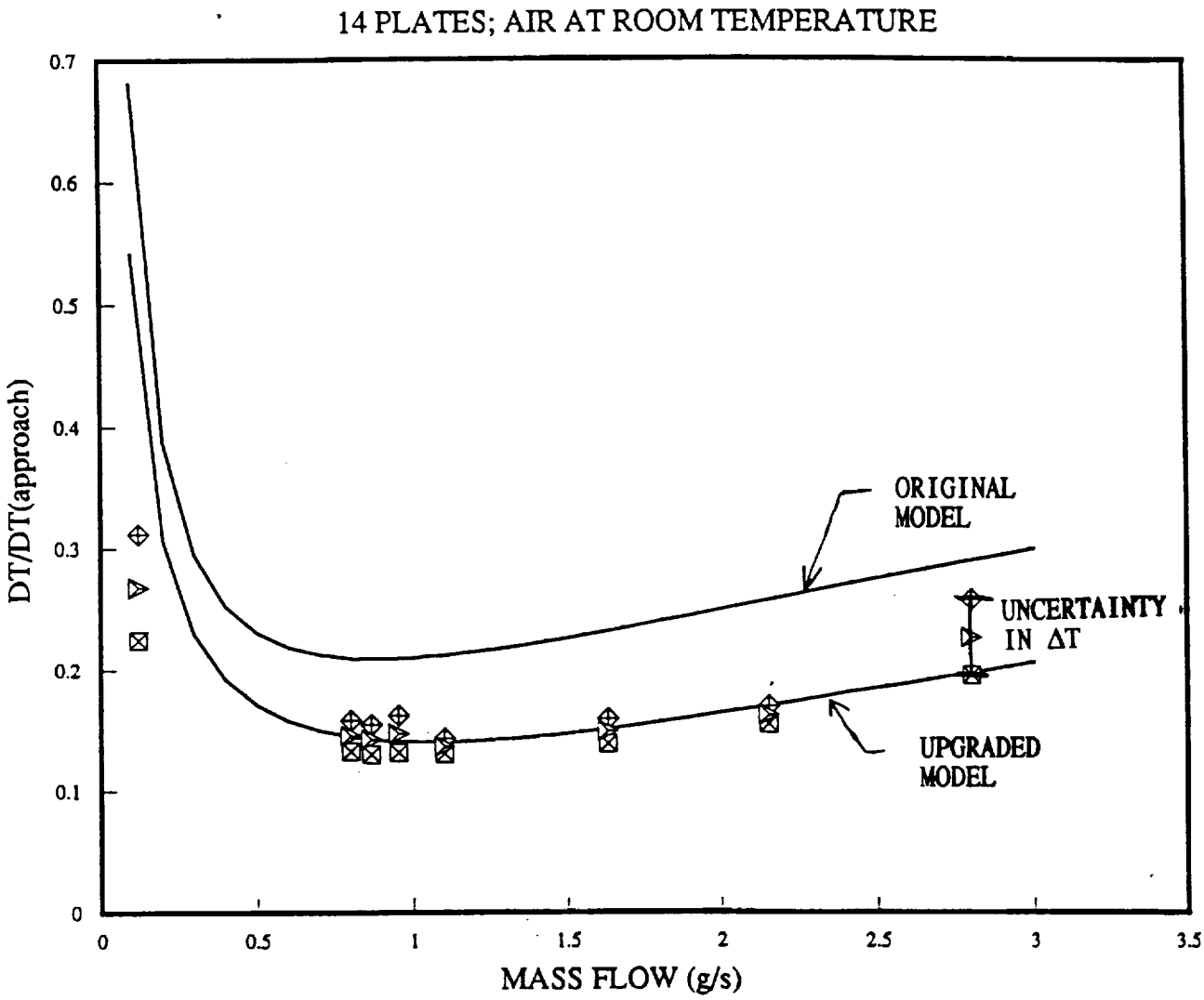

ORIGINAL MODEL

- GAS RESISTANCE ΔT ADDED TO FINITE # OF PLATES ΔT
- OUTER TUBE ATTACHED TO RINGS
- AVERAGE SLOT WIDTH

UPGRADED MODEL

- COMBINED MODELING OF GAS RESISTANCE AND FINITE # OF PLATES
- OUTER TUBE CONDUCTS ONLY BETWEEN HEADERS
- MINIMUM SLOT WIDTH

Figure 6.8 SLOT HEAT EXCHANGER THERMAL PERFORMANCE

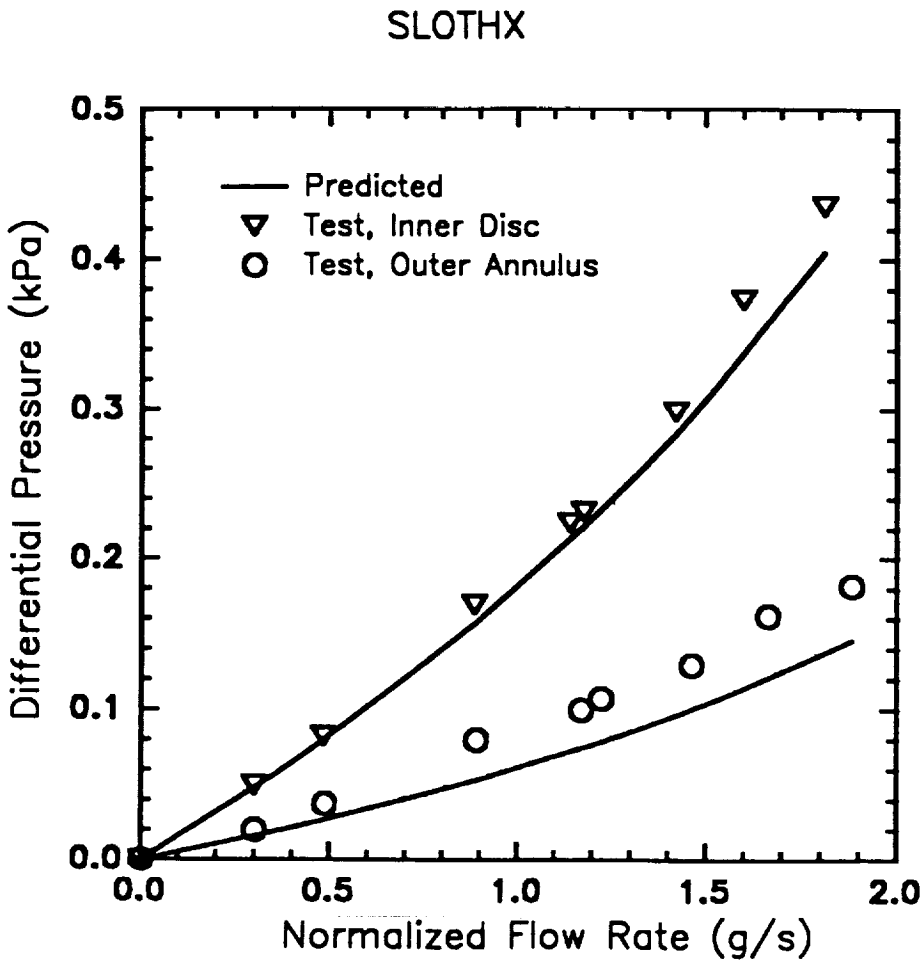

Figure 6.9 HEAT EXCHANGER PRESSURE LOSSES

Creare

The data points illustrate three interpretations of results. The diamonds give warm end ΔT's divided by the approach ΔT, squares are the cold end ΔT's divided by the approach ΔT, and the triangles are the averages of the two other values. Approach ΔT is the temperature difference through the length of the heat exchanger assembly (T_3 - T_1). The differences in ΔT warm and ΔT cold result from a combination of uncertainty in temperature measurement and heat leak from the heat exchanger to the ambient. The values at very low flow have relatively high uncertainty because of the inaccuracy in flow measurement. Over most of the test range, results are very consistent.

Figure 6.9 shows the performance of the test article in terms of pressure losses. The Figure contains test data and predicted pressure losses in each of the flow passages (the center passage through the disks and the annular passage containing rings) for room temperature air. The mass flow values on the abscissa are normalized to atmospheric pressure (during the tests, the internal pressure of the test article varied from test point to test point). The curves were generated using the same model used to predict performance of the heat exchanger. The test data were obtained in the third series of tests in which air temperature was uniform throughout. The model appears to underpredict pressure loss by about 3% in the inner flow passage and by about 20% in the outer passage.

The results of the tests were pleasing, both in the quality and consistency of the data and in the actual performance of the device. When the tests were first compared with predictions (from the original model) the differences were significant. The test results basically showed that the thermal losses were only two thirds of what had been expected. Our initial reaction was that there might be something fundamentally wrong with the tests. After reviewing the data and instruments, we examined the model used to predict the data. The tests allowed us to identify a few simplifying assumptions originally built into the model. The model was modified and was then able to corroborate the tests. The model was then rerun to evaluate how the full length heat exchanger would behave at design conditions. The result is that the thermal effectiveness for the full size heat exchanger is predicted to be 0.993. Pressure losses in the high pressure and low pressure streams are expected to be 3.1 kPa and 1.5 kPa, respectively. This results in an overall effectiveness of 0.99.

7. CONCLUSIONS

The key technology elements for a high performance, all-metal, compact heat exchanger have been developed and demonstrated. High performance in the compact configuration is achieved through the use of a large number small, precisely machined slots. All metal construction is achieved by mechanical positioning and soldering of disk and ring elements to tubes. A prototype test article embodying all important elements of the design was fabricated and tested. The thermal performance of the device exceeded original predictions and the thermal model was upgraded to reflect differences between original assumptions and the actual performance. The pressure losses in the test device slightly exceeded predictions. However, the overall performance of the heat exchanger is better than the original target. As a result of the improved performance in the heat exchanger, the overall cycle performance should be 20% better than predicted. This implies 20% less input power to the cycle for a fixed cooling load.

Creare

There are two remaining important steps in the adoption of this technology in a cryocooler. The most obvious is the construction of a full - up heat exchanger and testing at cryogenic temperatures. The second is the structural design and analysis to support the use of the heat exchanger in a system designed to meet space requirements. Although these two steps are important, they are in our opinion less challenging than the initial effort in developing the methods to accurately produce the slots.

8. REFERENCES

1. Valenzuela, J.A.; *All Metal Compact Heat Exchanger for Spaceborne Cryocoolers;* Creare TM-1107, August 1986.

2. Swift, W.L., Sixsmith, H., and Valenzuela, J.A.; *Long-Life, Closed-Cycle Cryocooler for Space;* Creare TN-413; Proceedings of the Fourth International Cryocoolers Conference, G. Green, ed., Easton MD: David Taylor Naval Ship R&D Center, September 1986, (July 1987), pp. 135-146.

3. Swift, W.L.; *A Reliable Long-Life, Closed-Cycle for Space*; Creare TN-455, presented at the Interagency meeting on Cryocoolers, Monterey, CA, August 1988.